f-f origin of the insulating state in uranium dioxide: X-ray absorption experiments and first-principles calculations

S.-W. Yu,[1,*] J. G. Tobin,[1] J. C. Crowhurst,[1] S. Sharma,[2] J. K. Dewhurst,[2] P. Olalde Velasco,[3,4] W. L. Yang,[3] and W. J. Siekhaus[1]

[1]*Lawrence Livermore National Laboratory, Livermore, California 94551, USA*

[2]*Max-Planck Institute for Microstructure Physics, Weinberg 2, Halle, Germany*

[3]*Advanced Light Source, Lawrence Berkeley National Laboratory, Berkeley, California 94720, USA*

[4]*Instituto de Ciencias Nucleares, UNAM, México, Distrito Federal 04510, México*

(Received 25 January 2011; published 4 April 2011)

We have performed x-ray absorption experiments on uranium dioxide (UO_2) at the O 1s, U 4d, U 4f, and U 5d edges. After comprehensive energy calibrations for O 1s, U 4d, and U 4f spectra, we have used the U 4d and 4f spectra to sort the energetic positions of the 5f and the 6d states in the unoccupied band unambiguously. This demonstrates conclusively that UO_2 is an f-f Mott-Hubbard insulator, where the electronic repulsion between f electrons is responsible for the insulating state. Calculations performed within the U-corrected generalized gradient approximation of the optical response of UO_2 permit direct comparison with the absorption spectra and confirm the experimental results.

DOI: 10.1103/PhysRevB.83.165102 PACS number(s): 71.30.+h

I. INTRODUCTION

The insulating phase of a Mott-Hubbard insulator is due to correlation effects associated with electron-electron interaction.[1] The properties of these insulators are substantially different from those of ordinary insulators described by noninteracting electrons in conventional band theory. When a charge carrier is excited across the Mott-Hubbard gap, both electrons and holes, in general, contribute to the electrical conductivity of Mott-Hubbard systems. However, due to the localization of the states involved, the effective mass of the excited electrons and holes are larger in such correlated systems compared to the uncorrelated systems, and therefore, the electrical conductivity is inhibited in the correlated systems. In a schematic way, the following exaggerated scenario is possible: In an ordinary insulator, if an energy corresponding to the band gap is provided, electrons are excited from the valence band to the conduction band and are delocalized, thereby contributing to the electrical conductivity of the material. However, in a Mott-Hubbard insulator of the f-f type, for example, if an energy corresponding to the band gap is provided, electrons are excited from one localized f state to another. Since the excited state is localized, the electron's contribution to the electrical conductivity is inhibited.

UO_2 is a known Mott-Hubbard insulator.[2] It is an important technological material since it is the principal fuel used in nuclear reactors for electrical power generation and research. In these systems it typically operates under conditions of high temperature and intense radiation.[3] A primary limitation of UO_2 as a fuel is its comparatively poor thermal conductivity.[2] A comprehensive understanding of the fundamental electronic structure of UO_2, which determines, at least in part, this and other relevant properties, is therefore desirable. More generally, precise experimental determination of the electronic structure provides an opportunity to rigorously test first-principles theoretical approaches developed to predict the properties of highly correlated systems.

The electronic structure of UO_2 has been the subject of several experimental and theoretical investigations over the last several decades. It has been studied using x-ray photoemission spectroscopy (XPS),[4–7] resonant photoemission spectroscopy (RPES),[8] optical absorption spectroscopy[9,10] inverse photoemission spectroscopy (IPES),[11] bremsstrahlung isochromat spectroscopy (BIS),[4] x-ray absorption spectroscopy (XAS),[12,13] and also theoretical methods.[13–20] Based on these experimental and theoretical results, much of the electronic structure of UO_2 has been clarified, but there are several important outstanding issues. One concern is the nature of the insulating state. As mentioned above, UO_2 belongs to a class of strongly correlated materials known as the Mott-Hubbard insulators, in which the electronic repulsion is responsible for the insulating state. However, it is not clear whether it is of f-f or f-d type. Optical measurement,[9,10] BIS,[4,5,17] and IPES[11] data suggested that UO_2 is f-d type, while O 1s XAS measurements[13] and theoretical calculations suggested that it is f-f type.[13,18–20] The distinction depends directly on the nature of the unoccupied state of UO_2. Since the top of the occupied states is dominated by f electrons, UO_2 is an f-f type insulator if the bottom of the unoccupied states is dominated by f character while it is f-d type if the bottom of the unoccupied states is dominated by d character.

To address the issue, we have performed XAS measurements not only at the O 1s, but also at the U 4f and U 4d edges. XAS is a powerful method of probing the unoccupied electronic states at a selected site.[12,13] In the O 1s XAS process, electrons from the 1s core level are excited to O 2p according to the dipole selection rules. In this case, O 2p is hybridized with U 5f and U 6d in the unoccupied state, and the O 1s XAS spectrum shows the hybridized characters between O 2p and U 5f and between O 2p and U 6d. In the case of the U 4f(4d) XAS process, electrons from U 4f(4d) are excited to 6d(5f) in the unoccupied state, respectively. Therefore, comparison between spectra measured at the different edges can provide directly the nature of the unoccupied state. Our data demonstrate experimentally and unambiguously that UO_2 is an f-f type Mott-Hubbard insulator. In parallel, we have performed calculations within the U-corrected generalized gradient approximation (GGA + U).

For GGA+U, we used the Perdew-Burke-Ernzerhof GGA functional as re-parameterized for solids, PBEsol.[21] The full potential linearized augmented plane wave (LAPW) method was used in conjunction with spin-orbit coupling, noncollinear magnetism, spin-polarized core states, and with a highly converged basis and k-point set. Parameters U = 4.772 eV and $J = 0.511$ eV were applied to U $5f$ to reproduce the experimental gap (about 2.1 eV, Refs. 4, 5). The deep lying O $1s$, U $4d$, and U $4f$ states were treated as part of the LAPW basis in the calculations which enabled us to compute the optical responses of the material over the entire energy range of the experiments (around 800 eV). Momentum matrix elements, used for determining the dielectric function ϵ, included the spin-orbit correction term.[22] The imaginary parts of ϵ (optical responses) are appropriately shifted to the conduction band minimum. These calculations were performed using the ELK code.[23] The remainder of the paper will describe in detail how this comparison and analysis was carried out.

II. EXPERIMENT

For the XAS measurements, a depleted $UO_2(100)$ single crystal of $\sim 3 \times 3$ mm^2 with thickness of $\sim$0.5 mm was prepared from a large crystal. Calculated mass and activity were $\sim$50 mg and $\sim$18.5 nanoCurie, respectively. Sample dimensions were chosen to minimize the activity while being consistent with the x-ray beam spot. XAS measurements were performed at Beam Line 8.0.1[24] of the Advanced Light Source at Lawrence Berkeley National Laboratory. The undulator and spherical grating monochromator provide linear polarized photons with resolving power ($E/\Delta E$) up to 6000. XAS spectra were accumulated by measuring the total fluorescent yield (TFY) and the total electron yield (TEY). The TFY is bulk sensitive compared to the TEY. Unless noted otherwise, the XAS spectra were normalized to the beam flux measured by a gold mesh (I_0). The resolution of the XAS measurement is estimated to be better than 0.3 eV. Low, medium, and high energy gratings are used for the XAS measurements. Supporting XPS and BIS measurements were carried out as described elsewhere,[25,26] on polycrystalline UO_2.

III. SPECTROSCOPIC RESULTS AND ENERGY CALIBRATION

The underlying processes of the four major spectroscopic measurements we performed are shown in Fig. 1: XPS of the valence bands and of the core levels, BIS or high energy inverse photoemission spectroscopy (IPES), and XAS. It is clear that these processes are interrelated but not identical. Both BIS and XAS should give some measure of the unoccupied density of states (UDOS) [i.e., the conduction bands (CB)]. However, by using the dipole selection rules and the elemental selectivity of XAS, the XAS should provide information concerning the elementally specific and orbital nature of the these states. Parallel to BIS, XPS of the valence bands should provide a measure of the occupied density of states (ODOS) [i.e., the valence bands (VB)]. XPS of the core levels will provide a means for the comparison of results using a "normalized energy" scale, as will be discussed below.

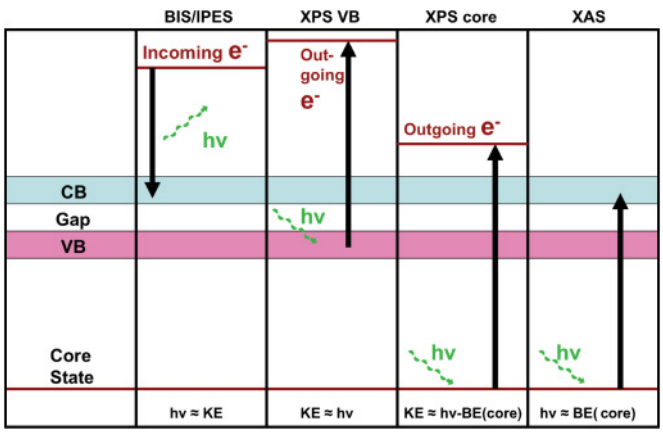

FIG. 1. (Color online) Sketch for the underlying processes of the major spectroscopic measurements performed in this paper: BIS, XPS, and XAS.

The XPS and BIS results for the VB and CB, respectively, are shown in Fig. 2. Although these two measurements have no intrinsic elemental specificity, there is a significant history of analysis, and the features within the VB have been assigned to various elementally specific states,[4–7,27,28] as we discussed in detail elsewhere.[25] Our VB and core level spectra of UO_2 are essentially identical with those reported earlier,[4–7,27,28] as is also true for our BIS measurement of UO_2.[4,5]

Three sets of XAS measurements of the O $1s$ are shown in Fig. 3, using first (nominal photon energy near 530 eV), second (nominal photon energy near 265 eV), and third order (nominal photon energy near 177 eV) soft x-rays. Because the energy selection of the beam line was performed using a spherical grating monochromator,[24] higher orders are possible. The medium energy grating was used for the data in Fig. 3. It was found that the energies of the three orders did not correspond to a simple ratio of 1:1/2:1/3, indicating some sort of small error in the grating calibration. A linear regression

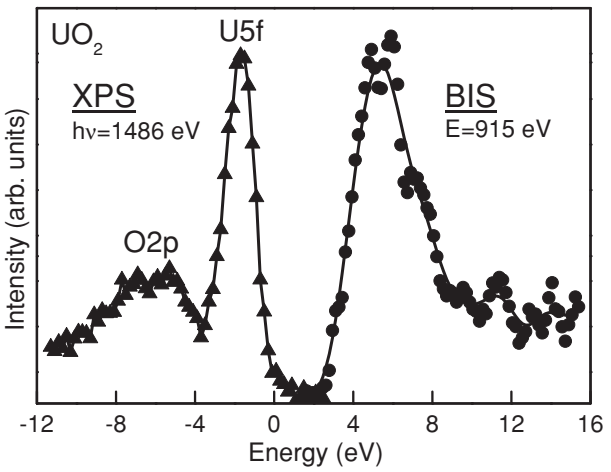

FIG. 2. A combination of XPS ($h\nu = 1486$ eV of photons) and BIS ($E = 915$ eV of electrons). For XPS, the reference point is the valence band maximum where the XPS spectrum ends. The BIS spectrum is lined up to the conduction band minimum after a band gap of 2.1 eV (Ref. 9). XPS and BIS measurements were performed with polycrystalline UO_2.

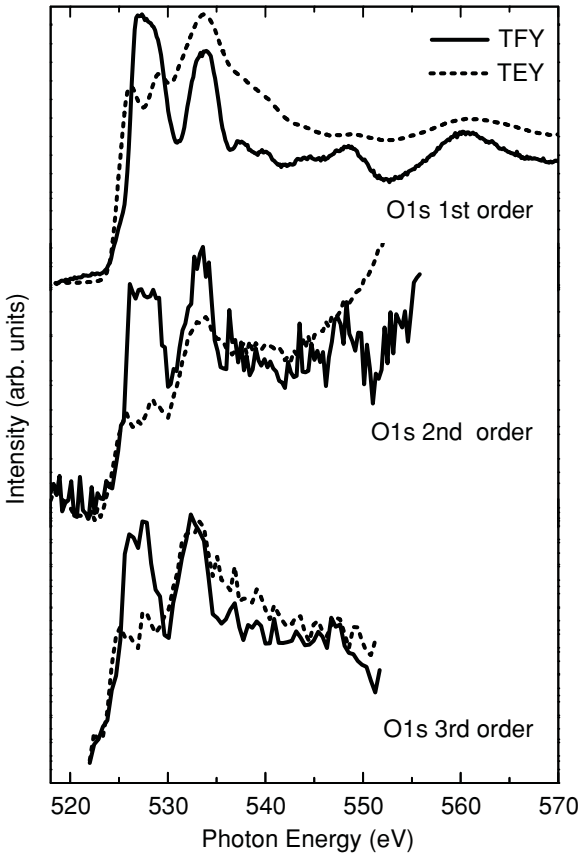

FIG. 3. O 1s XAS spectra using the first order, the second order, and the third order soft x rays. They are used for energy calibration for the medium energy grating. TFY and TEY are shown by solid line and short-dash, respectively. These XAS measurements were performed with a single crystal UO_2(100).

upon the observed energies was performed, giving rise to a single wavelength-correction, with $\Delta\lambda = 0.3$ angstroms, and an O 1s first maximum value of 527 eV. This single wavelength correction produces adjustments in energy space that scale with E^2 (from $E = h\nu = hc/\lambda$, $dE \propto d\lambda/\lambda^2$). While the appearance of the O 1s spectrum, in particular the TEY, was found to be essentially identical with earlier TEY results,[13] the energy of the first maximum had shifted from about 531 to 527 eV. However, considering the nature of the monochromator calibration herein, it is likely that the 527 eV energy is correct.

The uranium XAS spectra are shown in Fig. 4. The U $4d_{5/2}$ in both TFY and TEY, the U $4f_{7/2}$ in TFY only, and the U 5d in TFY only, are plotted. For the U $4f_{7/2}$, the medium energy grating was again used and the measured energy was subjected to the same energy correction, scaling with E^2, giving rise to the values shown in the middle panel of Fig. 4. The U 5d measured with the low energy grating was shown in the lower panel of Fig. 4. As it will be shown in Sec. IV, the U 5d spectrum cannot be used to characterize the unoccupied 5f states because the spin-orbit interaction of the 5d is smaller than the core-valence electrostatic interactions in the $5d \rightarrow 5f$ transition. But we show it just for comparison with previous data.[12] For the low energy grating, the energy calibration with the multiple order gratings was not possible

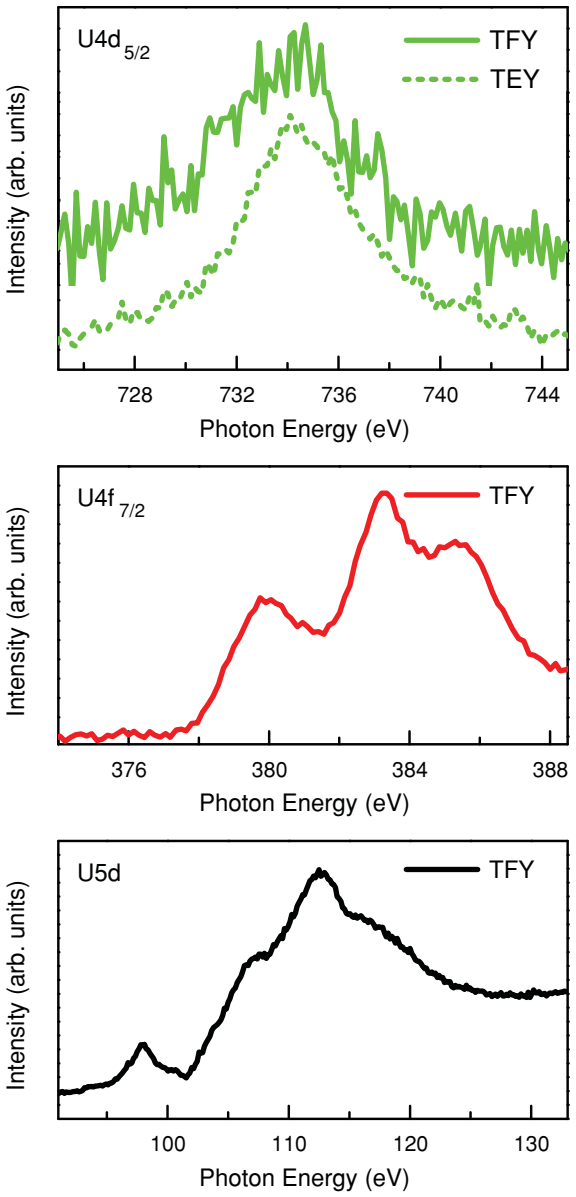

FIG. 4. (Color online) Upper panel: U $4d_{5/2}$ XAS in TFY and TEY. The spectra are normalized by I_0, which is measured by a gold mesh at the beam line. Middle panel: U $4f_{7/2}$ XAS in TFY. The spectrum is normalized by I_0. Lower panel: U 5d XAS in TFY. Unlike the cases of U $4d_{5/2}$ and U $4f_{7/2}$, this U 5d spectrum is not normalized by I_0 because of variations in I_0 over the photon energy range for the U 5d. This U 5d spectrum measured in TFY and without normalization by I_0 is consistent with the spectrum measured earlier in TEY mode (Ref. 12). These XAS measurements were performed with a single crystal UO_2(100).

due to the insufficient data. Therefore, the photon energy for U 5d has been shifted slightly to put it in agreement with earlier work.[12,32] The U $4d_{5/2}$ data was collected with the high energy grating and the spectrum itself and its energy were found to be consistent with earlier results for XAS of U and UF_4[12] and high energy EELS of UO_2.[29] Thus, no energy corrections were required for the U $4d_{5/2}$ data. The U $4f$ has been measured before: the high energy EELS (electron energy loss spectroscopy) data[30] for U are essentially the same as the

XAS herein. This argument is supported with the case study of Ce, where it was shown that high resolution, high energy EELS gives exactly the same result as XAS for both the Ce $4d$ and Ce $3d$ transitions.[31] The U $5d$ XAS has been reported earlier,[12,32] and our spectrum is in very good agreement with the TEY of UO_2 reported by Kalkowski *et al.*[12] In this earlier study, the surface was cleaned in ultrahigh vacuum. Thus, the presence of the U $5d$ XAS using TFY and absence of the U $5d$ XAS using TEY in our sample may reflect more surface degradation in our sample. (TEY is more surface sensitive than TFY, in general.)

Given the safety-related constraints that only a very small sample ($\sim 3 \times 3$ mm surface area) could be used, background variations and low signal rates are not unexpected. Due to refocusing optics, the vertical size of the x-ray spot was similar to the sample size and any misalignment could cause contributions from other materials such as the sample holder and sample supports. Thus, both the U $4f_{5/2}$ (N $1s$) and U $4d_{3/2}$ (Co $2p_{3/2}$) exhibited spectral interference. For this reason, neither of these are shown here. For the U $4f$ edges, the transitions were observed with TFY but not TEY. The observation of the U edges with TFY may reflect the onset of the dominance of x-ray fluorescence over Auger electron emission, in the decay process to fill the core holes induced by the x-ray absorption.[33,34] Thus, the issue of the weakness of the signal in TEY relative to TFY for the U $4f$ may not be merely a sample size (signal vs background) or surface effect. It may also reflect the different fundamental efficiencies of TFY vs TEY. As shown in Refs. 33 and 34, TFY gains relative to Auger as Z increases, at least for the K edge. Of course, there can be edge specific effects (e.g., the U $4d$ has a fairly strong TEY, the U $4f$ does not). Nevertheless, Auger emission drives TEY and x-ray emission is the source of TFY. The Z dependence helps to explain why the O $1s$ has both TEY and TFY and the U may be losing the TEY but not the TFY. (Finally, it should be noted that the U $4d$ transitions may be a special case, as evidenced by their unusually large lifetime broadening.)

A major point of this study is the issue of parentage of the UDOS. To resolve this issue, it is necessary to put all of the relevant XAS on the same energy scale. This problem is addressed in two separate ways: the normalized energy method and the threshold method.

First, the normalized energy scale will be introduced. One way to rectify all of the energies would be to subtract core level binding energies from the XAS energy scales. There is some concern about subtracting binding energies (from XPS) from photon energies (from XAS), because of the different final states and concomitant effects such as screening, shielding, relaxation, and so on. In XPS

$$(\text{Core})^a(\text{VB})^b(\text{CB})^0 + h\nu \rightarrow (\text{Core})^{a-1}(\text{VB})^b(\text{CB})^0 + e^-, \tag{1}$$

and in XAS

$$(\text{Core})^a(\text{VB})^b(\text{CB})^0 + h\nu \rightarrow (\text{Core})^{a-1}(\text{VB})^b(\text{CB})^1. \tag{2}$$

All of these effects appear to cancel out. However, the cancelation can be made more obvious by using the normalized energy, defined below, and subtracting a difference of XPS binding energies, which will remove any question of reference points in the measurements. Thus, we use 'normalized energy," which is essentially the O $1s$ photon energy. Normalized energy (NE) $= h\nu - [\text{BE} - \text{BE}(\text{O}1s)]$, where $h\nu$ is photon energy from XAS and BE is binding energy from XPS.[4,25] More specifically, for each edge

$$\text{NE}_{\text{O}1s} = h\nu(\text{O}1s), \tag{3}$$

$$\text{NE}_{\text{U}4f} = h\nu(\text{U}4f) - [\text{BE}(\text{U}4f) - \text{BE}(\text{O}1s)], \tag{4}$$

$$\text{NE}_{\text{U}4d} = h\nu(\text{U}4d) - [\text{BE}(\text{U}4d) - \text{BE}(\text{O}1s)]. \tag{5}$$

The result of this operation can be seen in Fig. 5. The U $4d_{5/2}$ peak has a huge lifetime broadening, giving rise to a Lorentzian, almost triangular, peak shape.[35] Thus, the U $4d_{5/2}$ threshold may well be in the center of the white line peak, consistent with the onset of the O $1s$ features. Here, one might raise the question of the disagreement with the earlier O $1s$ calibrations, such as that by Jollet *et al.*[13] However, to a certain extent, the point is moot. That is because the U $4f_{7/2}$ and O $1s$ peaks are both from the medium energy grating and thus

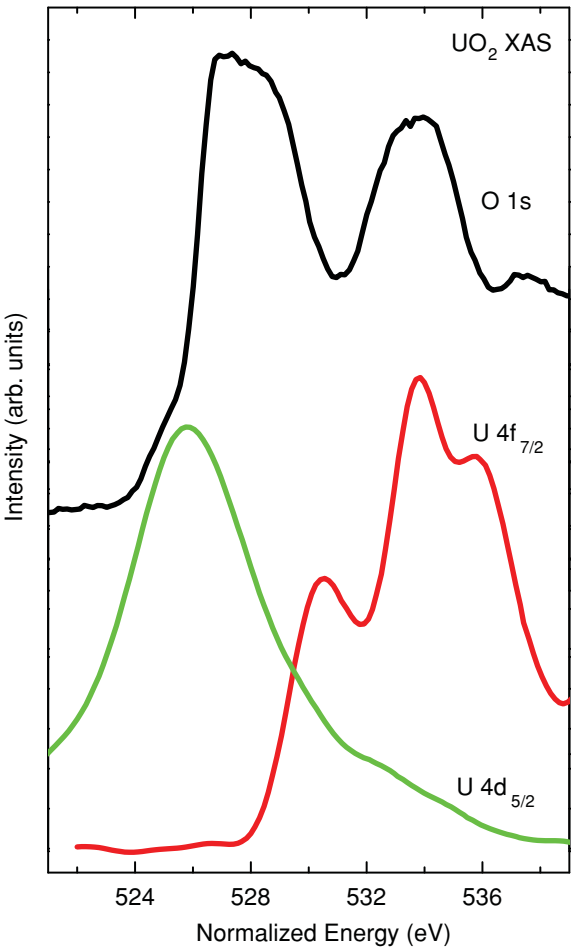

FIG. 5. (Color online) The alignment of O $1s$, U $4d_{5/2}$, and U $4f_{7/2}$, according to the energetic analysis [Eqs. (3), (4), and (5)]. O $1s$ and U $4f_{7/2}$ are shown in TFY mode while U $4d_{5/2}$ is shown in TEY mode. O $1s$ is from Fig. 3 (first order), without smoothing. U $4d_{5/2}$ is derived from U $4d_{5/2}$ TEY shown in the upper panel of Fig. 4, with seven points smoothing. U $4f_{7/2}$ is derived from U $4f_{7/2}$ TFY shown in the middle panel of Fig. 4, with five points smoothing.

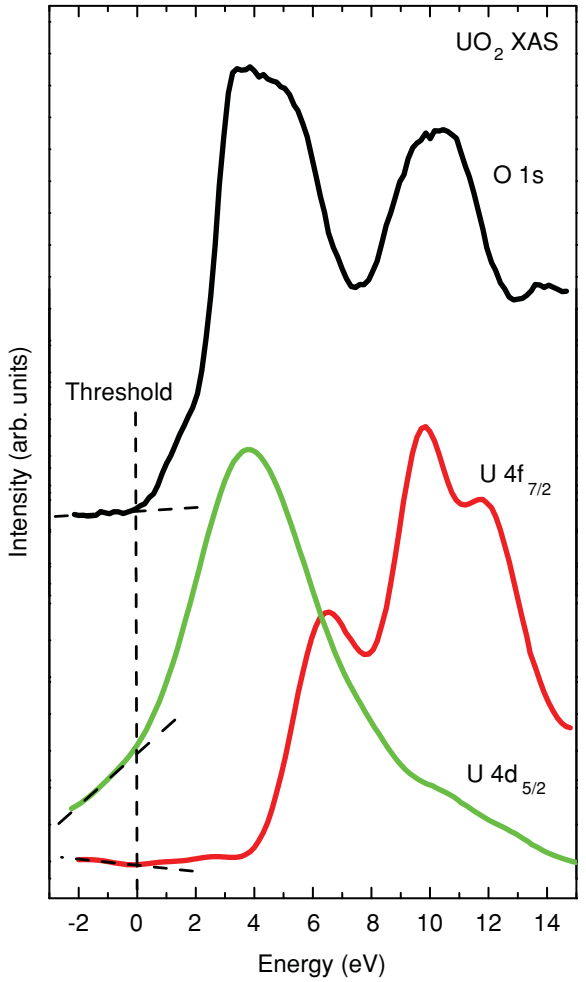

FIG. 6. (Color online) The alignment of O 1s, U 4$d_{5/2}$, and U 4$f_{7/2}$, according to the threshold analysis. O 1s and U 4$f_{7/2}$ are shown in TFY mode while U 4$d_{5/2}$ is shown in TEY mode. O 1s is from Fig. 3 (first order), without smoothing. U 4$d_{5/2}$ is derived from U 4$d_{5/2}$ TEY shown in the upper panel of Fig. 4, with seven points smoothing. U 4$f_{7/2}$ is derived from U 4$f_{7/2}$ TFY shown in the middle panel of Fig. 4, with five points smoothing.

tied together, while the U 4$d_{5/2}$ is from the high energy grating and thus separate. Recalibrating the O 1s will also move the U 4$f_{7/2}$. If an O 1s shift of 4 eV is performed, to bring it into agreement with Jollet *etal.*,[13] then the U 4$f_{7/2}$ moves with it proportionately and retains its relative position. All the while, the U 4$d_{5/2}$ remains at or near the O 1s onset.

An alternative independent approach is based upon a threshold analysis. In the U 4$d_{5/2}$ spectrum, there is a very strong lifetime broadening, which produces a Lorentzian peak shape. The threshold is probably directly under the centroid of the peak. However, if one were to take a contrarian viewpoint, one could define the threshold as the beginning of the peak spectral intensity. Then one could align all of the spectra based upon the thresholds, arguing that this represents the conduction band minimum. If one follows through on this analysis, the result in Fig. 6 is obtained, which is almost identical to the result in Fig. 5.

IV. SPECTROSCOPIC ANALYSIS, COMPARISON TO THEORY AND UDOS

The upper panel of Fig. 7 shows the XPS, BIS, and XAS results obtained by lining up on the valence band maximum and the conduction band minimum. The assignments for the peaks of O 1s XAS are given according to Ref. 13. The four peaks measured are assigned as a through d. To account for this spectrum, we need to understand the hybridization between O 2p and U 5f(6d) in the unoccupied state. Through the hybridization,

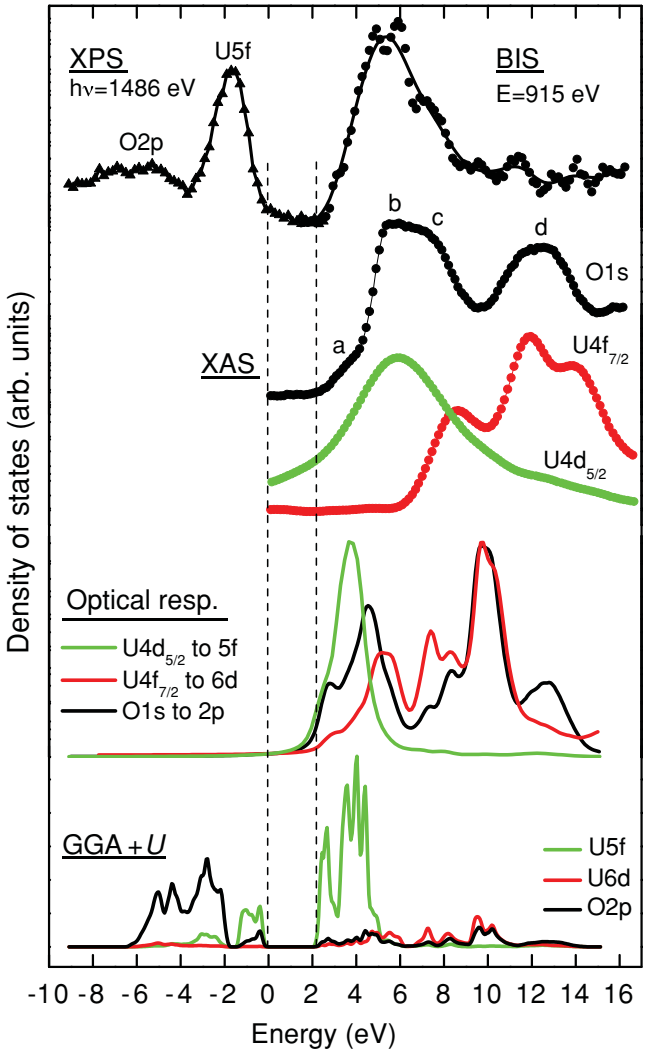

FIG. 7. (Color online) Upper panel: A combination of XPS, BIS, and XAS. The XPS and BIS are lined up on the valence band maximum and the conduction band minimum with a band gap of 2.1 eV as shown in Fig. 2. XAS spectra of O 1s, U 4$d_{5/2}$, and U 4$f_{7/2}$ are lined up to the conduction band minimum after the threshold analysis (Fig. 6). O 1s and U 4$f_{7/2}$ are shown in TFY mode while U 4$d_{5/2}$ is shown in TEY mode. For the O 1s XAS spectrum, the structures a and b originate from the hybridization between O 2p and U 5f, while the structures c and d originate from that between O 2p and U 6d. Middle panel: Optical responses (imaginary parts of dielectric function) for the core levels of O 1s, U 4$d_{5/2}$, and U 4$f_{7/2}$. Bottom panel: GGA + U calculations for O 2p, U 6d and U 5f partial DOS. Parameters $U = 4.772$ eV and $J = 0.511$ eV were applied to U 5f.

O $2p$ electrons transfer to the unoccupied U $5f(6d)$ state and there is the possibility that O $1s$ electrons can be excited to the empty O $2p$ state in the XAS process governed by the dipole selection rules $\Delta\ell = \pm 1$. Therefore, it is evident that without the hybridization, there would not exist such a structure in O $1s$ XAS because O $2p^6$ is filled completely within an ionic bonding picture and cannot accommodate additional electrons.

UO_2 is composed of U^{4+} and O^{2-} and its ground state configuration can be written as U $6p^6 5f^2 6d^0 7s^0$ O $2p^6$ ($5f^2$ configuration).[13] When hybridization between oxygen and uranium is activated, the $5f^2$ configuration is coupled with $5f^3\underline{L}$ and $5f^2 6d^1\underline{L}$ configurations ($\underline{L}$ denotes a hole in O $2p$), where $5f^3\underline{L}$ ($5f^2 6d^1\underline{L}$) denotes the configuration obtained from $5f^2$ by transferring an O $2p$ electron to the $5f$ ($6d$) state. Only one hole in O $2p$ has been considered, and configurations involving $7s$ states are neglected. With hybridization, therefore, the ground state becomes a combination of $5f^2$, $5f^3\underline{L}$, and $5f^2 6d^1\underline{L}$ configurations. During the O $1s$ XAS process, an O $1s$ electron is excited to the empty O $2p$ level. This implies that after x-ray absorption, the lowest-energy final states accessible are mixtures of $\underline{c}5f^3$ and $\underline{c}5f^2 6d^1$ configurations ($\underline{c}$ denotes a hole in O $1s$). If we neglect the hybridization between $5f$-$6d$ as it is expected to be small,[13] one can consider that O $1s$ XAS will consist of the two types of configurations of $\underline{c}5f^3$ and $\underline{c}5f^2 6d^1$.

The structures a and b in the O $1s$ XAS shown in the upper panel of Fig. 7 can be attributed to the $\underline{c}5f^3$ configuration.[13] In fact, the first-principles calculations based on the LSDA + U (Ref. 13) and the hybrid density-functional theory,[14] as well as our calculations shown in the bottom panel of Fig. 7 (GGA + U) show that the unoccupied $5f$ states are lower in energy than the unoccupied $6d$ states. Furthermore, for the $5f^3$ electronic interactions, both the spin-orbit splitting and the cubic crystal-field splitting are approximately 1 eV (Refs. 13, 15). These electronic interactions of the spin-orbit splitting and the cubic crystal-field splitting lead to a very complex multiplet structure that may spread over several eV for $5f^3$ states, producing the structures a and b in O $1s$ XAS. Therefore, the structures a and b reflect the $5f^3$ multiplet states hybridized with O $2p$ states.

Next we consider the $\underline{c}5f^2 6d^1$ configuration. Under a cubic crystal-field symmetry, $6d$ states are split into the two-fold degenerate e_g and the three-fold degenerate t_{2g} states.[9,10] The e_g states are lower in energy than the t_{2g} states. If we neglect the spin-orbit coupling of $6d$ states and the $5f$-$6d$ interaction, there is no $6d$ multiplet interaction because there is only one $6d$ electron. Therefore, the possible configurations are $5f^2 6e_g^1$ and $5f^2 6t_{2g}^1$, which can be attributed to the structures c and d, respectively, in the O $1s$ XAS shown in the upper part of Fig. 7. The energy separation between the structures c and d is 4.3 eV, which is in agreement with the 4.4 eV energy splitting between $6d(e_g)$ and $6d(t_{2g})$ in UO_2 found within a multiple scattering approach.[36] Therefore, the structures c and d are attributed to U $6d(e_g)$ and U $6d(t_{2g})$ states split by the cubic crystal-field, hybridized with O $2p$ states.

Our O $1s$ XAS spectrum measured in TFY mode from a single crystal UO_2 is in agreement with previous O $1s$ XAS data measured in TEY mode from polycrystalline UO_2 (Ref. 13), and confirms that the U $5f$ state is located lower in energy than the U $6d$ state in the unoccupied band. Therefore, UO_2 can be classified as an f-f Mott-Hubbard insulator.[18] But it is in disagreement with other findings,[4,11,17] in which UO_2 is classified as an f-d type insulator based on optical, BIS, and IPES measurements.

So far, we have used only theory to analyze the O $1s$ XAS spectrum, which argues for an f-f type insulating nature of UO_2. This conclusion is still ambiguous as the energetic positions of the unoccupied $5f$ and $6d$ states could be switched in reality. Is there any way to confirm the f-f nature of UO_2 on the basis of XAS experimental data alone? One way is to excite other core electrons to the unoccupied states of $5f$ and $6d$ (e.g., to perform $d \rightarrow 5f$ and $f \rightarrow 6d$ XAS measurements). For the $d \rightarrow 5f$ XAS, in principle, both the core levels U $5d$ and U $4d$ can be used. But the spin-orbit interaction of the core level $5d$ is smaller than the core-valence electrostatic interactions in the $5d \rightarrow 5f$ transition, and this effectively smears out the transitions, encapsulating both the $5d_{5/2} \rightarrow 5f$ and $5d_{3/2} \rightarrow 5f$ peaks within the giant resonance, thus making identification of the $5f$ in the unoccupied state[12] difficult (as also shown in the lower panel of Fig. 4). We, therefore, selected the $4d \rightarrow 5f$ transition.

As shown in the upper panel of Fig. 7, the U $4d_{5/2} \rightarrow 5f$ XAS shows features at the energy positions of the structures a and b measured in O $1s$ XAS. However, although it is not clear to rule out the presence of peak c, peak d is not present. This results from the fact that the structures a and b originate from the f character of the unoccupied states. To detect the d character of the unoccupied states, we used the U $4f_{7/2} \rightarrow 6d$ XAS. In this case, the U $4f_{7/2} \rightarrow 6d$ XAS spectrum[37] does not show any features at the positions of the structures a and b, but shows features at the positions of structures c and d, which are derived from the d character. Therefore, the combination of the $4d \rightarrow 5f$ and $4f \rightarrow 6d$ XAS measurements, with O $1s$ XAS, as shown in the upper panel of Fig. 7, is conclusive experimental evidence that the $5f$ state is located lower in energy than $6d$ in the unoccupied states of UO_2, and that UO_2 is an f-f Mott-Hubbard insulator.

The suggestion of an f-d type insulator is mainly based on optical measurements[10] and the interpretation of the BIS data.[4] We first consider the optical measurements. As shown in the upper panel of Fig. 7, it is well known from the XPS data of UO_2[4,6,8] that the occupied valence band of UO_2 is composed of both the O $2p$ band, which tails off at approximately -4 eV relative to the VBM, and the occupied U $5f$ state, which lies at about -1.5 eV relative to the VBM. In the optical measurement, the O $2p$ and the U $5f$ electrons are excited to the unoccupied states, obeying the dipole selection rules. Therefore, neither the O $2p$ nor the U $5f$ electrons can access the unoccupied $5f$ state. They can only access the unoccupied $6d$ state. In fact, the first-principles calculations of the electronic structure of UO_2, which include correlation effects,[13,14,16,19] and our calculations of GGA + U shown in the bottom panel of Fig. 7 indicate clearly that the unoccupied U $5f$ and U $6d$ states coexist and furthermore, the onset of the two unoccupied states occurs at about the same energy above the band gap, but the DOS of the unoccupied U $5f$ state is several hundred times stronger than that of the U $6d$ state at the position of the onset. The DOS of the U $5f$ state is predominant at the bottom of the unoccupied states and the DOS of the U $6d$ is relatively extremely small, but not zero. This might explain

why the f-d type is suggested on the basis of the optical measurement. Second, the suggestion of f-d type based on the BIS measurement[4] arose from the interpretation of a shoulder, assigned to the U 6d state, at the beginning of the BIS spectrum. However, if we take the fact into account that the cross section for the f state is dominant at the high energy used for BIS measurement,[38] it becomes implausible that the shoulder originated from the 6d state. In fact, in our BIS measurement with electron energy of 915 eV shown in the upper panel of Fig. 7, the feature and the energetic position of the BIS spectrum are similar to the U $4d_{5/2} \rightarrow 5f$ XAS. This means that the f state is dominant already at the energy of 915 eV.

We note that pure UO_2 is known to be a good insulator [conductance at room temperature is approximately 4×10^{-3} $(\Omega\text{cm})^{-1}$][39] with a band gap of only 2.1 eV (Ref. 9), which is comparable with other common semiconductors. Therefore, conceptually, the f-f type is preferred over the f-d type to explain the insulating nature of UO_2. If UO_2 had a f-d type band gap, the d state, being more delocalized in the conduction band, would contribute more to the conductivity than the f state, and UO_2 would be a semiconductor.

As can be seen from Fig. 7, the GGA + U results and the corresponding optical responses agree well with the experimental results and previous calculations,[13,14] and imply that UO_2 is an f-f Mott-Hubbard insulator.

Finally, in light of these results, it would be desirable to comprehensively characterize the electronic structure that determines the insulating nature of the higher oxides of uranium. XPS studies indicate that the intensity of the U $5f$ peak located near the VBM is decreased as the oxidization increases, and even disappears in UO_3.[6] Clearly, as the oxidation increases, more electrons are transferred from the U $5f$ to the O $2p$ states.

In conclusion, O 1s XAS data show that O $2p$ and U $5f$(6d) hybridize in the unoccupied states and produce the complex structure in O 1s XAS of UO_2. The hybridization between O $2p$ and U $5f$ is responsible for the structure in the lower energy region, and the hybridization between O $2p$ and U 6d is responsible for the structure in the higher energy region of the O 1s x-ray absorption spectra of UO_2. The U $4d \rightarrow 5f$ and U $4f \rightarrow$ 6d XAS provide conclusive experimental evidence that the $5f$ state is located lower in energy than 6d in the unoccupied state, and that UO_2 is an f-f Mott-Hubbard insulator. This result is also confirmed by our GGA + U theoretical calculations.

ACKNOWLEDGMENTS

We would like to thank Ian Hutcheon, Patrick Allen, Anthony Van Buuren, Trevor Wiley, and Joseph Zaug for valuable discussion. POV would like to acknowledge CONACyT México. Lawrence Livermore National Laboratory is operated by Lawrence Livermore National Security, LLC, for the U.S. Department of Energy, National Nuclear Security Administration under Contract No. DE-AC52-07NA27344. This work is funded by Laboratory Directed Research and Development (LDRD) Program No. (10-SI-016) of Lawrence Livermore National Laboratory. Some of the work performed by JGT and SWY was supported by the DOE Office of Science, Office of Basic Energy Science, Division of Materials Sciences and Engineering. The Advanced Light Source (ALS) is supported by the Director, Office of Science, Office of Basic Energy Sciences, of the U.S. Department of Energy under Contract No. DE-AC02-05CH11231.

*Corresponding Author: YU21@LLNL.GOV

[1] M. Imada, A. Fujimori, and Y. Tokura, Rev. Mod. Phys. **70**, 1039 (1998).
[2] Q. Yin and S. Y. Savrasov, Phys. Rev. Lett. **100**, 225504 (2008).
[3] R. J. McEachern and P. Taylor, J. Nucl. Mater. **254**, 87 (1998).
[4] Y. Baer and J. Schoenes, Solid State Commun. **33**, 885 (1980).
[5] Y. Baer, Physica B+C **102**, 104 (1980).
[6] B. W. Veal and D. J. Lam, Phys. Lett. A **49**, 466 (1974).
[7] B. W. Veal and D. J. Lam, Phys. Rev. B **10**, 4902 (1974).
[8] L. E. Cox, W. P. Ellis, R. D. Cowan, J. W. Allen, S.-J. Oh, I. Lindau, B. B. Pate, and A. J. Arko, Phys. Rev. B **35**, 5761 (1987).
[9] J. Schoenes, J. Appl. Phys. **49**, 1463 (1978).
[10] J. Schoenes, Phys. Rep. **63**, 301 (1980).
[11] P. Roussel, P. Morrall, and S. J. Tull, J. Nucl. Mater. **385**, 53 (2009).
[12] G. Kalkowski, G. K. Kaindl, W. D. Brewer, and W. Krone, Phys. Rev. B **35**, 2667 (1987).
[13] F. Jollet, T. Petit, S. Gota, N. Thromat, M. Gautier-Soyer, and A. Pasturel, J. Phys. Condens. Matter. **9**, 9393 (1997).
[14] K. N. Kudin, G. E. Scuseria, and R. L. Martin, Phys. Rev. Lett. **89**, 266402 (2002).
[15] A. Hasegawa and H. Yamagami, Prog. Theor. Phys. Suppl. **108**, 27 (1992).
[16] S. L. Dudarev, D. Nguyen Manh, and A. P. Sutton, Philos. Mag. B **75**, 613 (1997).
[17] O. Gunnarsson, D. D. Sarma, F. U. Hillebrecht, and K. Schönhammer, J. Appl. Phys. **63**, 3676 (1988).
[18] A. Kotani and T. Yamazaki, Prog. Theor. Phys. Suppl. **108**, 117 (1992).
[19] Q. Chen, X. Lai, T. Tang, B. Bai, M. Chu, Y. Zhang, and S. Tan, J. Nucl. Mater. **401**, 118 (2010).
[20] L. E. Roy, T. Durakiewicz, R. L. Martin, J. E. Peralta, G. E. Scuseria, C. G. Olson, J. J. Joyce, and E. Guziewicz, J. Comput. Chem. **29**, 2288 (2008).
[21] J. P. Perdew, A. Ruzsinszky, G. I. Csonka, O. A. Vydrov, G. E. Scuseria, L. A. Constantin, X. Zhou, and K. Burke, Phys. Rev. Lett. **100**, 136406 (2008).
[22] H. Rathgen and M. I. Katsnelson, Phys. Scr. T **109**, 170 (2004).
[23] [http://elk.sourceforge.net/].
[24] J. J. Jia, T. A. Callcott, J. Yurkas, A. W. Ellis, F. J. Himpsel, M. G. Samant, J. Stohr, D. L. Ederer, J. A. Carlisle, E. A. Hudson, L. J. Terminello, D. K. Shuh, and R. C. C. Perera, Rev. Sci. Instrum. **66**, 1394 (1995).
[25] S.-W. Yu and J. G. Tobin, J. Vac. Sci. Technol. A **29**, 021008 (2011).
[26] J. G. Tobin, S.-W. Yu, B. W. Chung, G. D. Waddill, E. Damian, L. Duda, and J. Nordgren, Phys. Rev. B **83**, 085104 (2011).

[27] A. Goldmann, T. Ishii, R. Manzke, J. R. Naegele, and M. Skibowski, in *Landolt-Bornstein: Numerical Data and Functional Relationships in Science and Technology, Group III*, Vol. 23b, edited by A. Goldmann (Springer-Verlag, Berlin, 1994).

[28] G. C. Allen, I. R. Trickle, and P. M. Tucker, Philos. Mag. B **43**, 689 (1981).

[29] K. T. Moore, G. van der Laan, R. G. Haire, M. A. Wall, and A. J. Schwartz, Phys. Rev. B **73**, 033109 (2006).

[30] H. R. Moser, B. Delley, W. D. Schneider, and Y. Baer, Phys. Rev. B **29**, 2947 (1984).

[31] K. T. Moore, B. W. Chung, S. A. Morton, A. J. Schwartz, J. G. Tobin, S. Lazar, F. D. Tichelaar, H. W. Zandbergen, P. Söderlind, and G. van der Laan, Phys. Rev. B **69**, 193104 (2004).

[32] P. van Kampen, Ch. Gerth, M. Martins, P. K. Carroll, J. Hirsch, E. T. Kennedy, O. Meighan, J.-P. Mosnier, P. Zimmermann, and J. T. Costello, Phys. Rev. A **61**, 062706 (2000).

[33] G. Ertl and J. Kueppers, *Low Energy Electrons and Surface Chemistry* (Verlag Chemie, Weinheim, 1974).

[34] K. Siegbahn, *ESCA Applied to Free Molecules* (North Holland, Amsterdam, 1969).

[35] J. G. Tobin, P. Söderlind, A. Landa, K. T. Moore, A. J. Schwartz, B. W. Chung, M. A. Wall, J. M. Wills, R. G. Haire, and A. L. Kutepov, J. Phys. Condens. Matter **20**, 125204 (2008).

[36] J. Guo, D. E. Ellis, E. Alp, L. Soderholm, and G. K. Shenoy, Phys. Rev. B **39**, 6125 (1989).

[37] The detailed structure of the U $4f_{7/2} \rightarrow 6d$ XAS spectrum remains to be explained, but is outside of the scope of this work.

[38] T. Fauster and F. J. Himpsel, Phy. Rev. B **30**, 1874 (1984).

[39] M. R. Castell, C. Muggelberg, G. A. D. Briggs, and D. T. Goddard, J. Vac. Sci. Technol. B **14**, 966 (1996).